Nanoscale

COMMUNICATION

View Article Online
View Journal

Cite this: DOI: 10.1039/c9nr01688k

Received 25th February 2019,
Accepted 24th May 2019

DOI: 10.1039/c9nr01688k

rsc.li/nanoscale

Development of an image biosensor based on an optogenetically engineered cell for visual prostheses

Gongxin Li, [a,b,c] Feifei Wang,[d] Wenguang Yang, [e] Jia Yang,[a,b,f] Yuechao Wang,[a,b] Wenxue Wang*[a,b] and Lianqing Liu *[a,b]

Visual prostheses provide blind patients with artificial vision *via* electrical stimulation of surviving visual cells resulting in partial restoration of vision in many patients. However, high-resolution visual perception, long-term biocompatibility and safety remain the significant challenges of existing visual prostheses. Here, we present a novel method to develop a new visual prosthesis using living cells as integrated electronics and implantable microelectrodes. The living cells modified with channelrhodopsin-2 showed excellent light-sensitive properties and encoded image information with cellular deformations triggered by light stimulation. The photoresponsive properties of the cells were determined using a single pixel imaging system, which indicated that the cells can act as a good light-sensitive biosensor. Additionally, the imaging feasibility of the cells was further validated through successful and clear imaging of several object scenes using the same system. This work represents a step toward the design and use of living cells as an image biosensor for the development of a new generation of high-resolution visual prostheses.

1. Introduction

Blindness is one of the most feared disabilities that poses extraordinary challenges to individuals and has impacted millions of people worldwide. Although pharmacological interventions and molecular genetics techniques have provided some effectiveness at slowing down the progression or have provided therapeutic solutions to visual damage, currently, there remains a lack of effective treatments for many patients who are visually impaired because of damage to the retina, optic nerves or visual parts of the brain.[1,2] Thus, visual prostheses are viable rehabilitative and therapeutic options to substitute and eventually restore useful visual sensation by electrically stimulating the surviving neural cells in the visual system.[3–6] However, high-resolution visual perception, long-term biocompatibility and safety still remain the main technical challenges in the development of visual prostheses.

Visual prostheses, which typically consist of electronics to process image and generate stimulus pulses and implantable microelectrode arrays to stimulate the retina, provide stable, portable and long-term visual cell stimulation inducing visual perceptions that allow blind patients to form recognition.[7,8] Several visual prostheses, such as Argus I,[9] Argus II,[6] Alpha IMS[10] and EPIRET3,[11] have been tested in clinical trials as a potential treatment method for blind patients. The current visual prostheses allow blind patients to precept light stimulation, and, therefore, be capable of localizing objects, identifying letters, recognizing sample shape and detecting motion after long-term training.[6,12] However, the visual acuity of such artificial prostheses remains much lower than the normal value for the criteria of legal blindness (<20/200). One of the main reasons for this difference is that it is difficult to achieve high-density microelectrode arrays within a very small space. The visual prostheses do not provide normal vision but rather a series of marginal and irregular spots that comprise the contours of visual perception; thus, the spatial resolution of the contours is determined by the density of the microelectrode array. For example, Argus II has only 60 microelectrodes and Alpha IMS has 1500 independent stimulators,[13,14] with which the maximal visual acuities are only 20/1260 [6] and 20/546,[12] which are lower than the criterion value for legal blindness. Therefore, patients wearing such prostheses are still legally blind. Furthermore, each microelectrode provides an independent stimulus channel interfaced with the surviving visual

[a]State Key Laboratory of Robotics, Shenyang Institute of Automation, Chinese Academy of Sciences, Shenyang 110016, China. E-mail: lqliu@sia.cn, wangwenxue@sia.cn
[b]Institutes for Robotics and Intelligent Manufacturing, Chinese Academy of Sciences, Shenyang 110016, China
[c]Key Laboratory of Advanced Process Control for Light Industry (Ministry of Education), Institute of Automation, Jiangnan University, Wuxi 214122, China
[d]Department of Chemistry, Stanford University, Stanford, California 94305, USA
[e]School of Electromechanical and Automotive Engineering, Yantai University, Yantai 264005, China
[f]University of Chinese Academy of Sciences, Beijing 100049, China

neural cells. On the one hand, the interactions between neural cells and molecules at the outer surfaces of microelectrodes are prone to acute or chronic inflammatory reactions, which often result in damage to visual neurons and to the surfaces of the microelectrodes;[1,15] on the other hand, there are also challenges in that the stimulus requires a sustained and strong energy supply while minimizing the prosthesis size.[16]

In principle, the above issue faced by the visual prosthesis can be circumvented by the use of light-sensitive living cells as integrated electronics and implanted microelectrodes. Such cells have ultrahigh biocompatiblity and therefore do not cause any damage to visual neural cells. Furthermore, a light-sensitive living cell utilizes available local nutrients to supply continuous and long-term energy for a visual stimulus. Thus, we herein explore a novel method to develop a new visual prosthesis using living cells as integrated electronics and implanted microelectrodes. The cells are genetically modified to express the opsin of channelrhodopsin-2 (ChR2) as an image biosensor. The opsin is bound by retinal and constructs the retinal–opsin complex, which undergoes photoisomerization after the absorption of the photons and produces obvious cellular deformation measured by atomic force microscopy (AFM),[17] as shown in Fig. 1(a). The properties of the cells integrate the dual functions of the electronics and implanted microelectrodes in a visual prosthesis, because the cells can transform the light stimulation into a mechanical response to process image and stimulate the retina.

To determine the photoresponsive properties and validate the imaging performance of the cells, a single-pixel imaging system was designed and built, as shown in Fig. 1(b). The system consists of three primary components: (i) an AFM system, which provides a readout of the photoresponsive information of the cells after the absorption of the photons, (ii) an optical microscope containing a CCD, red light and an objective, which is used to observe and guide the manipulation and measurement of the AFM, and (iii) a stimulating light structure consisting of a light spatial modulator (digital micromirror device, or DMD), light of wavelength of 470 nm and an object image, integrated in the optical microscope by a beamsplitter and used to stimulate the targeted cell with the light. The stimulating light structure uses DMD to adjust the light intensity irradiated on the cell.

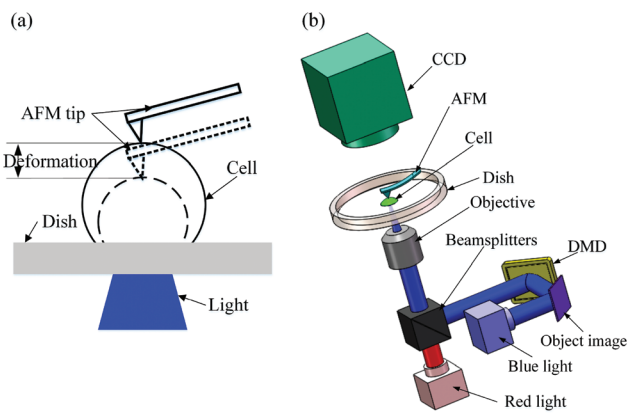

Fig. 1 (a) Overview of the cellular photoresponsive properties and the measurement method; (b) schematic diagram of the single pixel imaging system.

2. Results and discussion

Optogenetics is an approach that allows targeted, fast and precise control of the defined events in specific cells of living tissue by combining genetic and optical methods.[18–20] The genetic method is used to encode proteins that can be targeted to specific cell subtypes, and the optical method is used to interrogate these proteins to gain or inhibit their actions. Furthermore, in fact, these encoded proteins are opsins that incorporate retinal, a vitamin A-related organic photon-absorbing cofactor, to enable light sensitivity.[21] The retinal chromophore will be isomerized and trigger a series of structural changes, which results in ion channel opening or closing after the absorption of the photons. Additionally, the state changes of a large number of the ion channels inevitably lead to cell contraction or relaxation.[17,22] Thus, if the cellular deformation of the optogenetically engineered cell, which describes the contraction and relaxation of the cell, can be triggered after the absorption of the photons, it is also considered a sensitive probe to represent visual information.

We explored the cellular deformation upon absorption of the photons to characterize the photoresponsive performance of the optogenetically engineered cells. The cell type used in this work were Human Embryonic Kidney 293 (HEK293) cells expressing the ChR2 protein fused with an enhanced yellow fluorescent protein based on the report of G. Nagel,[23] as shown in Fig. 2(a). Cells with green fluorescence indicate successful expression of ChR2, and the patch-clamp was also used for further validation due to the observation of large photocurrents after the absorption of the photons.

An LED light (470 nm, <10 mW mm^{-2}) was chosen to confirm the direct activation of the ion channels of the cells and the light was designed and adjusted so as to target a single cell (Fig. 2(b)). The experimental result indicated that the ChR2-expressing cells triggered cellular deformations under light irradiation (3.9 mW mm^{-2}), as shown in Fig. 2(c). Large cellular deformations were observed after light irradiation and the cells become smaller due to the contraction of the cellular membrane. Control measurements, including the AFM probe tip which is not in contact with the ChR2-expressing cells (Fig. 2(d)) and the AFM probe tip which in contact with the cells not expressing ChR2 (the result is the same as that shown in Fig. 2(d)), were used to exclude the possibility that the cellular deformation is triggered by the temperature variation generated by the light irradiation and prove that cellular deformation is truly evoked by the ChR2-expressing cell upon absorption of the photons, because almost any change of the cellular deformation in the control measurements is observed. Additionally, Young's modulus, which is a measurement of the stiffness of a viscoelastic material, was

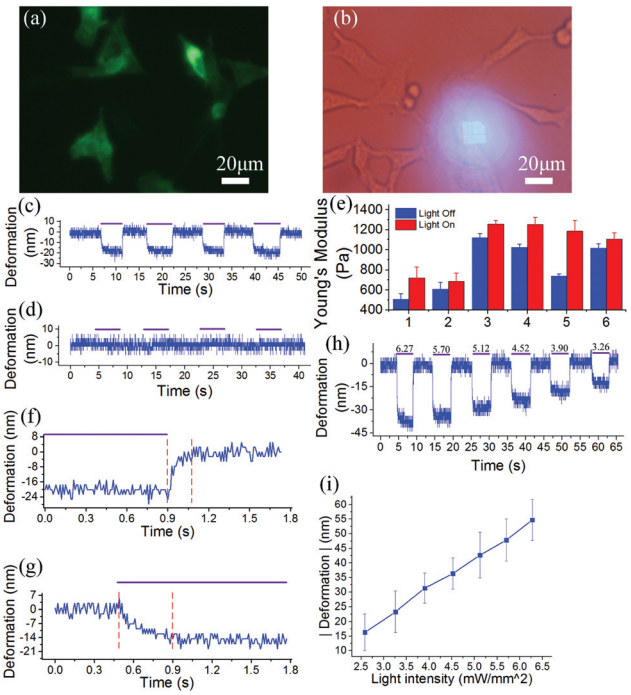

Fig. 2 Cellular deformations of ChR2-expressing cells. (a) Fluorescence image of HEK293 cells expressing ChR2, (b) Image showing the light targeted to a single cell, (c, d) Cellular deformations under light irradiation with the same light intensity at different times when the probe tip of the AFM comes into contact with the cell surface (c) and when it is not in contact with the cell (d), n = 10 cells, (e) Young's modulus of the cell before and after light irradiation; the X axis denotes different cells; (f, g) the delayed relaxation of cellular deformations before and after light on (f) or off (g), n = 10 cells, (h) cellular deformations under light irradiation with different light intensities, (i) cellular deformation output recorded from a cell as a function of the light applied to the cell, n = 10 cells. Note: The purple lines represent the period when the light is on.

also measured and calculated for further validation of the cellular deformation properties of the cell. Fig. 2(e) shows that the Young's modulus of the cell after the absorption of the photons is larger than that of the cell in the dark. And it reveals that the stiffness of the cell increases after the absorption of the photons because the increase in the Young's modulus of the cell is caused by cell contraction, which is generated by the cumulative effect of the opening of many of the ion channels.

Because living cells are generally considered viscoelastic materials with viscoelastic creep behavior,[24,25] delayed relaxation occurs after cellular deformation induced by light irradiation. The delayed relaxation time during which the cell membrane recovered to the saturated state (or desensitization time) was up to 180 ± 21 ms with the light off (Fig. 2(f)). And the activation time of the cell was approximately 450 ± 34 ms with the light on, as shown in Fig. 2(g). The sum of the desensitization time and the activation time demonstrated that the time of light stimulation was at least 630 ± 29 ms if the cell reaches a stable state after the absorption of the photons and the light responsive speed of the cell was approximately 1.59 s^{-1}.

As demonstrated above, cellular deformation is generated by the cumulative effect of the opening or closing of mass ion channels triggered by the light. The size of the cellular deformation was proportional to the number of activated ion channels, and was affected by the intensity of the light irradiated on the cell. Fig. 2(h) shows that the amplitude of the cellular deformations is affected by the input light power and the cellular deformation decreases with the reduced input light power. The size of the cellular deformation was directly proportional with the input light power, as shown in Fig. 2(i), which validates that the HEK293 cell expressing ChR2 can be used as a fine light-sensitive sensor, and the cell can transform the light stimulation information into a mechanical-responsive signal.

To demonstrate that the cells have the ability to transform visual information under view into a mechanical signal to stimulate the retina for the design of a new generation of visual prosthesis, the imaging performance of the cells was validated by imaging several object images using the single-pixel imaging system. The three letters 'S', 'I' and 'A' were used as object scenes under the view, as shown in Fig. 3(a), for the imaging experiment, the resolution of all the recovered images was set at 50 × 50 pixels, and the images were reconstructed from only 750 measurements, which is only 30% of the total number of pixels. In this study, a commercial photodiode (OPT 101, Texas Instruments Inc., USA) was also used as the light-sensitive sensor to test the implementation of the optical system of the single-pixel imaging system in the function of imaging and compared the imaging performance with that using the ChR2-expressing cell. The recovered images using

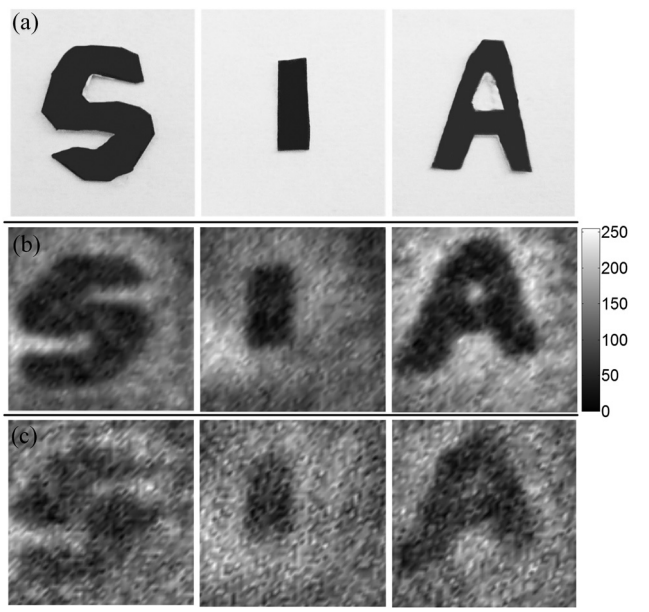

Fig. 3 Imaging results. (a) Object scenes ('S', 'I' and 'A') used to test the imaging feasibility of a single living ChR2-expressing cell. Only the spatial information corresponding to the white patches was sampled and carried by the light irradiated onto the cell, (b) images recovered using the commercial photodiode (OPT101), (c) images recovered using the cell.

the commercial photodiode, as shown in Fig. 3(b), indicate that the optical system of a single-pixel imaging system is feasible, because the recovered images can clearly detect the contour of the object images. Fig. 3(c) presents the images recovered by the cell using the same single-pixel imaging system and shows that the contour of the object images can also be significantly distinguished. The results confirm that the optogenetically engineered cell can perceive visual information and transform it into a mechanical signal to stimulate the retina.

3. Conclusions

The photoresponsive properties of ChR2-expressing HEK293 cells are presented above and indicate that cells can act as a light-sensitive biological sensor. The successful imaging of several object scenes validates that these cells have similar function to the integration of electrons and implantable microelectrodes of a visual prosthesis, that is, they process image information and generate stimulus signals and stimulate the retina. It is difficult for a cell to maintain long-term stability because of the variation in the physiological state of the cell. Thus, the images obtained by the image biosensor were inferior to those by the photodiode. However, compared with the current visual prostheses, the main information exchange medium between the biological sensor and surviving visual cells is biological information, which allows the cell to have excellent biocompatibility and safety in a visual prosthesis. Being able to utilize local nutrients allows the cell to provide a long-term stimulus to visual cells without any additional energy supply requirement. Moreover, the imaging acquisition results for some object scenes validate the feasibility of using cells for imaging in visual prostheses. Additionally, the imaging resolution of the image biosensor is much higher than that of the existing visual prostheses. This study reveals a new method to use image biosensors as integrated electronics and implanted microelectrodes of a visual prosthesis. In the future, we will attempt to fabricate a large-scale array of image biosensors to increase the imaging speed and reduce system complexity, thereby increasing the potential to develop a new generation of visual prostheses.

4. Materials and methods

4.1. Cell preparation

Human embryonic kidney 293 (Hek293) cells were cultured in a complete culture medium, including high glucose Dulbecco's modified Eagle's medium (DMEM, Thermo Scientific Inc., USA) supplemented with 10% fetal bovine serum (FBS, ExCell Bio Inc., USA) and 1% penicillin–streptomycin (Thermo Scientific Inc., USA) solution, at 37 °C with 5% ambient CO_2 in a 60 mm^2 dish. When the cells were more than 90% confluent, they were used to transfect the ChR2 plasmid, which was constructed based on the report of G. Nagel.[23] Before expressing ChR2, a mixed solution of the ChR2 plasmid and the transfection reagent (Lipofectamine 2000, Thermo Scientific Inc., USA) was prepared. First, 0.5 mL DMEM without FBS is used to dilute 8 μg ChR2 plasmid and 20 μL transfection reagent in a centrifuge tube, and then, the tube was shaken gently and incubated for 5 minutes at room temperature. Second, the plasmid dilution and transfection reagent dilution were mixed well and placed for 20 minutes at room temperature. Third, the cells were washed using phosphate buffered saline (PBS) and DMEM solution without FBS once, respectively, and 3 mL DMEM solution without FBS was added into the dish. Fourth, the mixed solution of the plasmid and transfection reagent was added to the dish, and the cells were incubated for 6 hours at 37 °C with 5% ambient CO_2. Finally, the medium of the cells was replaced with 4 mL complete culture medium and was persistently incubated for 24 hours. Next, the cells were used as an experimental sample.

4.2. Measurement of cellular deformations

First, to mimic the physiological environment of cells *in vitro* and accurately measure the cellular deformations, an external recording solution was prepared in advance. The external recording solution comprised the following: 140 mM NaCl, 1 nM$GaCl_2$, 2 nM $MgCl_2$ and 10 nM HEPES. Second, before measuring cellular deformation, the opsin of encoded ChR2 should be incorporated into the retinal; this opsin–retinal complex was referred to rhodopsin. Thus, 4 μL retinal solution was added to the ChR2-expressing cells, and then the cells were incubated for 30 minutes at 37 °C with 5% ambient CO_2. Third, the solution in the dish was discarded, and then the cells were washed using PBS and the external recording solution once each. Next, 4 mL external recording solution was added to the dish. Next, the sample was completely prepared.

Next, the dish was placed on the stage of the AFM system (Bruker Bioscope, Catalyst Inc., USA). The stimulating light structure is adjusted to guarantee that the light targeted a single cell. The AFM probe tip is guided to the cell surface, where the best location is the highest point of the cell, by optical microscopy. The probe tip was pressed on the cell surface and stopped. Finally, the cellular deformations were measured using the AFM system when the input light powers were adjusted by the DMD.

4.3. Scheme of the single-pixel imaging system

The single-pixel imaging system is based on the mathematical theory and reconstruction algorithms of compressive sensing,[26,27] which combines both sampling and compression in a linear measurement process and recovers scenes under the view using the after-treatment optimization.[28,29] The center of compressive sensing is to recover a sparse signal $x \in R^N$ from an observation vector $y \in R^M$ and a measurement matrix $\Phi \in R^{M\times N}$ using the linear equation: $y = \Phi x$, where $M < N$.[30,31] Although the equation is under-determined, the unique solution $\hat{x}$ is also obtained if the x is sparse enough and the measurement matrix satisfies the restricted isometry property (RIP).[32,33] In practice, not all signals are sparse in

their original form, but they can be sparsely represented in other spaces.

The single-pixel imaging system is the typical application of the compressive sensing theory and contains a light source, lens, digital micromirror device (DMD), light-sensitive sensor and signal acquisition system, as shown in Fig. 1(b). DMD, as the core component of the single-pixel imaging system, consists of an array of square micromirrors, each of which can be positioned at two angles, −12° and +12°, and turned along the diagonal. The positions of the DMD are controlled by a random picture of 1024 × 768 pixels, and each micromirror is independently controlled by the corresponding pixel value of either 1 or 0. If the pixel value is 1, the corresponding micromirror is positioned at −12°, otherwise it is positioned at +12°. The light can be reflected on the sensor only on the +12° position of micromirrors. Any random picture is patterned by a corresponding row of the measurement matrix Φ. Upon all micromirrors of the DMD being controlled by a random picture, a measurement can be obtained. Repeating the turn M times, the observation vector y with length of M is acquired. Finally, the recovered image can be reconstructed from y and Φ using optimization algorithms. Here, the light-sensitive sensor is the ChR2-expressing cell and the signal acquisition system is the AFM system.

The single-pixel imaging system, rather than collecting pixel samples of an objective image under the view, measures the inner products between the object image and the measurement matrix function. It converts the object image with a space-series signal into a time-series signal, and each measurement for the single is a sum of pixel value taken across the entire image.[26,27] The conversion is realized *via* the measurement matrix function and the signal is measured by the HEK293 cells expressing ChR2, as a special light-sensitive biosensor in the single-pixel imaging system.

Conflicts of interest

There are no conflicts to declare.

Acknowledgements

This work was supported by the National Key R & D Program of China (Grant No. 2018YFB1304700), the Natural Science Foundation of Jiangsu Province of China (Grant No. BK20180592), the National Natural Science Foundation of China (Grant No. 91748212, U1613220, U1813210, 91848201, 61573341, 61727811) and the Key Research Program of Frontier Sciences, CAS (Grant No. QYZDB-SSW-JSC008).

References

1 E. Fernandez and R. Normann, in *Introduction to Visual Prostheses*, ed. H. Kolb, E. Fernandez and R. Nelson, University of Utah Health Sciences Center, Salt Lake City, 2016.
2 J. D. Weiland and M. S. Humayun, *Proc. IEEE*, 2008, **96**, 1076–1084.
3 J. D. Weiland, W. Liu and M. S. Humayun, *Annu. Rev. Biomed. Eng.*, 2005, **7**, 361–401.
4 S. Picaud and J. A. Sahel, *C. R. Biol.*, 2014, **337**, 214–222.
5 L. Bareket, A. Barriga-Rivera, M. P. Zapf, N. H. Lovell and G. J. Suaning, *J. Neural. Eng.*, 2017, **14**, 045002.
6 M. S. Humayun, J. D. Dorn, L. da Cruz, G. Dagnelie, J. A. Sahel, P. E. Stanga, A. V. Cideciyan, J. L. Duncan, D. Eliott, E. Filley, A. C. Ho, A. Santos, A. B. Safran, A. Arditi, L. V. Del Priore, R. J. Greenberg and A. I. S. Grp, *Ophthalmology*, 2012, **119**, 779–788.
7 J. D. Weiland and M. S. Humayun, *IEEE Trans. Biomed. Eng.*, 2014, **61**, 1412–1424.
8 L. da Cruz, B. F. Coley, J. Dorn, F. Merlini, E. Filley, P. Christopher, F. K. Chen, V. Wuyyuru, J. Sahel, P. Stanga, M. Humayun, R. J. Greenberg, G. Dagnelie and for the Argus II Study Group, *Br. J. Ophthalmol.*, 2013, **97**, 632–636.
9 M. S. Humayun, J. D. Weiland, G. Y. Fujii, R. Greenberg, R. Williamson, J. Little, B. Mech, V. Cimmarusti, G. Van Boemel, G. Dagnelie and E. de Juan, *Vision Res.*, 2003, **43**, 2573–2581.
10 E. Zrenner, K. U. Bartz-Schmidt, H. Benav, D. Besch, A. Bruckmann, V. P. Gabel, F. Gekeler, U. Greppmaier, A. Harscher, S. Kibbel, J. Koch, A. Kusnyerik, T. Peters, K. Stingl, H. Sachs, A. Stett, P. Szurman, B. Wilhelm and R. Wilke, *Proc. Biol. Sci.*, 2011, **278**, 1489–1497.
11 G. Roessler, T. Laube, C. Brockmann, T. Kirschkamp, B. Mazinani, M. Goertz, C. Koch, I. Krisch, B. Sellhaus, H. K. Trieu, J. Weis, N. Bornfeld, H. Rothgen, A. Messner, W. Mokwa and P. Walter, *Invest. Ophthalmol. Visual Sci.*, 2009, **50**, 3003–3008.
12 K. Stingl, K. U. Bartz-Schmidt, D. Besch, A. Braun, A. Bruckmann, F. Gekeler, U. Greppmaier, S. Hipp, G. Hortdorfer, C. Kernstock, A. Koitschev, A. Kusnyerik, H. Sachs, A. Schatz, K. T. Stingl, T. Peters, B. Wilhelm and E. Zrenner, *Proc. Biol. Sci.*, 2013, **280**, 20130077.
13 S. Rizzo, C. Belting, L. Cinelli and L. Allegrini, *Graef. Arch. Clin. Exp.*, 2015, **253**, 323–325.
14 K. Stingl, K. U. Bartz-Schmidt, D. Besch, C. K. Chee, C. L. Cottriall, F. Gekeler, M. Groppe, T. L. Jackson, R. E. MacLaren, A. Koitschev, A. Kusnyerik, J. Neffendorf, J. Nemeth, M. A. Naeem, T. Peters, J. D. Ramsden, H. Sachs, A. Simpson, M. S. Singh, B. Wilhelm, D. Wong and E. Zrenner, *Vision Res.*, 2015, **111**, 149–160.
15 G. C. McConnell, H. D. Rees, A. I. Levey, C. A. Gutekunst, R. E. Gross and R. V. Bellamkonda, *J. Neural. Eng.*, 2009, **6**, 056003.
16 M. Javaheri, D. S. Hahn, R. R. Lakhanpal, J. D. Weiland and M. S. Humayun, *Ann. Acad. Med.*, 2006, **35**, 137–144.
17 G. X. Li, J. Yang, Y. C. Wang, W. X. Wang and L. Q. Liu, *Nanoscale*, 2018, **10**, 21046–21051.
18 K. Deisseroth, *Nat. Neurosci.*, 2015, **18**, 1213–1225.
19 K. Deisseroth, *Nat. Methods*, 2011, **8**, 26–29.
20 E. S. Boyden, F. Zhang, E. Bamberg, G. Nagel and K. Deisseroth, *Nat. Neurosci.*, 2005, **8**, 1263–1268.

21 F. Zhang, J. Vierock, O. Yizhar, L. E. Fenno, S. Tsunoda, A. Kianianmomeni, M. Prigge, A. Berndt, J. Cushman, J. Polle, J. Magnuson, P. Hegemann and K. Deisseroth, *Cell*, 2011, **147**, 1446–1457.
22 T. Bruegmann, T. van Bremen, C. C. Vogt, T. Send, B. K. Fleischmann and P. Sasse, *Nat. Commun.*, 2015, **6**, 7153.
23 G. Nagel, T. Szellas, W. Huhn, S. Kateriya, N. Adeishvili, P. Berthold, D. Ollig, P. Hegemann and E. Bamberg, *Proc. Natl. Acad. Sci. U. S. A.*, 2003, **100**, 13940–13945.
24 P. Pravincumar, D. L. Bader and M. M. Knight, *PLoS One*, 2012, **7**, e43938.
25 F. M. Hecht, J. Rheinlaender, N. Schierbaum, W. H. Goldmann, B. Fabry and T. E. Schaffer, *Soft Matter*, 2015, **11**, 4584–4591.
26 M. F. Duarte, M. A. Davenport, D. Takhar, J. N. Laska, T. Sun, K. F. Kelly and R. G. Baraniuk, *IEEE Signal Proc. Mag.*, 2008, **25**, 83–91.
27 G. Li, W. Wang, Y. Wang, W. Yang and L. Liu, *Opt. Express*, 2016, **24**, 400–408.
28 R. G. Baraniuk, *IEEE Signal Proc. Mag.*, 2007, **24**, 118–124.
29 G. Li, P. Li, Y. Wang, W. Wang, N. Xi and L. Liu, *Int. J. Optomechatroni.*, 2014, **8**, 218–227.
30 E. J. Candes and M. B. Wakin, *IEEE Signal Proc. Mag.*, 2008, **25**, 21–30.
31 G. Li, W. Wang, Y. Wang, S. Yuan, W. Yang, N. Xi and L. Liu, *IEEE Trans. Nanotechnol.*, 2015, **14**, 837–846.
32 E. J. Candes, *CR. Math.*, 2008, **346**, 589–592.
33 G. Li, J. Yang, W. Yang, Y. Wang, W. Wang and L. Liu, *Remote Sens.*, 2017, **9**, 619.

